PSFC/JA-02-28

Edge Dimensionless Experiment on DIII-D and Alcator C-Mod

D.A. Mossessian, R.J. Groebner[1], R.A. Moyer[2], T.H. Osborne[1],
J.W. Hughes, M. Greenwald, A. Hubbard, T.L. Rhodes[3]

November 2002

Plasma Science and Fusion Center
Massachusetts Institute of Technology
Cambridge, MA 02139 USA

[1]General Atomics, PO Box 85608, San Diego, CA 92186
[2]University of California, San Diego, San Diego, CA 92121
[3]University of California, Los Angeles, Los Angeles, CA 90095

Submitted for publication to *Physics of Plasmas*.

Edge dimensionless identity experiment on DIII-D and Alcator C-Mod.

D. A. Mossessian

MIT, Plasma Science and Fusion Center, Cambridge, MA 02139

 R. J. Groebner

General Atomics, PO Box 85608, San Diego, CA 92186

R. A. Moyer

University of California, San Diego, San Diego, CA 92121

T. H.Osborne

General Atomics, PO Box 85608, San Diego, CA 92186

J. W. Hughes, M. Greenwald, A. Hubbard

MIT, Plasma Science and Fusion Center, Cambridge, MA 02139

T. L. Rhodes

 University of California, Los Angeles, Los Angeles, CA 90095

Abstract

Experiments were carried out to study the similarity of H-mode (High confinement mode) physics on the Alcator C-Mod [1] and DIII-D [2] tokamaks comparing plasmas with matched local edge dimensionless parameters (β, $\rho*$, $\nu*$, q_{95}) and shape (ε, κ, δ). It was observed that matching local values of the dimensionless parameters on top of the H-mode pedestals produces similar T_e and n_e profiles across the entire pedestal region, with pedestal width scaling linearly with the machine size. Furthermore, in H-modes with matched pedestals, similar edge fluctuations were observed. Discharges in DIII-D with scaled pedestal parameters similar to those of C-Mod EDA (Enhanced D-alpha) H-mode showed a quasicoherent mode localized to the outer half of the pedestal, similar to the C-Mod quasicoherent mode (QC mode). The wavenumber of the mode observed on DIII-D matches the wavenumber of the C-Mod QC mode if scaled with the machine size. For higher pedestal temperatures and pressures, small high frequency ELMs (Edge Localized Modes) appear in both machines.

I. Introduction.

For standard H-mode (High confinement mode) discharges, experimental evidence shows that there is a strong correlation between global plasma confinement and the local plasma parameters at the top of the H-mode pedestal [3,4,5,6,7]. Thus, in order to obtain a more complete understanding and a predictive capability for core confinement, it is necessary to also understand the physics of the structure of the H-mode pedestal. At this time, the physics of the H-mode pedestal is not sufficiently well understood to allow for predictions of how its parameters should scale between machines. One potentially powerful approach to improving this understanding would be to apply techniques of dimensionless identity, which have been used in studies of core plasmas [8,9], to study the physics of the pedestal region. These techniques are based on the fundamental fact that the governing equations of plasma physics can be made dimensionless by introducing three characteristic parameters (collisionality, normalized plasma pressure β, and normalized gyroradius) [10,11,12,13]. Conservation of values of these dimensionless parameters would then imply the invariance of physics with respect to changes of the dimensional parameters. In other words, the discharges produced on tokamaks of different sizes with different plasma parameters but identical dimensionless parameters should demonstrate similar physics.

A first step in such studies would be to perform an "identity" experiment, in which it would be determined if the appropriate dimensionless parameters could be matched on the pedestals of two different machines. If such an identity could be achieved at the top of the pedestal, it would be of interest to see if the identity match could be maintained throughout the pedestal. Due to the presence of sources and sinks in the pedestal region, which are generally ignored in dimensional studies, it is not clear that identity throughout the entire pedestal would be possible. If the plasma physics identity could be maintained throughout the entire pedestal, then any phenomena that depend purely on plasma physics should be observed in both machines.

In this paper we describe the results of an identity experiment carried out on Alcator C-Mod [1] and DIII-D [2] tokamaks. In these experiments, plasmas with identical local edge dimensionless parameters were created in tokamaks with a geometrical size ratio of 2.5, and with different core heating mechanisms – ICRH (Ion cyclotron Radiation Heating) on C-Mod and neutral beam heating on DIII-D. It was argued in Ref. 12 that for a dimensionless identity experiment the compared discharges should have the same shape of heating power deposition profile and the same distribution of power deposition between electrons and ions. It has been shown, however, that temperature profiles in tokamak plasmas react only weakly to changes in the heating deposition profile [3,14,15]. Instead, the temperature profiles are self-consistent and the energy transport adjusts to maintain a certain minimum temperature gradient scale length in the plasma core, with the temperature at the pedestal serving as a boundary condition. This profile self-similarity is also predicted by some theories, for example, by ITG (Ion Temperature Gradient) turbulence model [16]. This suggests, that to create dimensionally similar discharges in different tokamaks only the power flow across the separatrix, which defines local edge temperature, should be scaled with the geometrical size of

the machine and not the net input power, and the profile and mechanism of power deposition in the core should not be too important.

The strategy of the experiment is described in the next section. The results show, that despite the differences in the heating mechanisms, similar edge profiles can be obtained on both machines when power flow across the separatrix is scaled appropriately. It was also found that, although the core profiles of temperature and density in the discharges with similar edges are not similar, this difference can be explained by an additional core fueling source on DIII-D tokamaks (neutral beam fueling). At the same time, the global transport and confinement characteristics are similar on both machines, as expected. The global parameters of the similar plasmas are compared in Section III of the paper.

Atomic processes such as ionization, impact excitation and charge exchange whose rates depend mainly on plasma temperature should play a significant role in edge pedestal formation.. Characteristic lengths of the atomic processes will not scale with the machine size if only the plasma physics dimensionless parameters are matched. Therefore, since the ion flux at the edge should be balanced by the local source provided by ionization of the neutral influx, matching local edge dimensionless parameters should not produce similar H-mode pedestal characteristics, except by coincidence, if diffusive ion transport is assumed. However, the results presented in this paper indicate that pedestal profiles do match quite well on both machines. Although we cannot present a clear theoretical explanation of the results at this moment, several possible explanations exist, which are discussed in Section IV of the paper.

Finally, dimensional identity of the edge profiles should lead to similar edge stability characteristics, suggesting that similar character of H-mode should be observed on both machines. Indeed, similarity of the edge fluctuations was observed in discharges with matched edge profiles, with a quasicoherent mode present in the edge of the DIII-D discharge similar to EDA (Enhanced D-alpha) C-Mod H-mode, and small grassy ELMs (Edge Localized Modes) observed in both plasmas under similar edge conditions. These results are presented in Section V.

II. Scaling of plasma parameters

The dimensionless parameters that need to be matched for the solutions of the plasma equations to be similar are collisionality (the ratio of electron-ion collision frequency to the bounce frequency), normalized ion gyroradius the (ratio of ion gyroradius and the characteristic plasma size), and normalized pressure (the ratio of kinetic and magnetic pressure) [12]:

$$\nu^* \sim \frac{a n_e}{T_e^2} \qquad (1)$$

$$\rho^* \sim \frac{\sqrt{T_e}}{B_t a} \qquad (2)$$

$$\beta \sim \frac{n_e T_e}{B_t^2} \qquad (3)$$

Here a is the plasma minor radius, n_e and T_e are electron density and temperature respectively, and B_t is the toroidal magnetic field. The similarity of magnetic topology is achieved by matching the safety factor profile, taking into account that the scaling of the local value of the safety factor at the plasma edge can be expressed as:

$$q_{95} \sim \frac{aB_t}{I_p} \qquad (4)$$

Finally, the shape parameters - elongation κ, upper and lower triangularity $\delta_{u,l}$, and inverse aspect ratio

$$\varepsilon = a/R \qquad (5)$$

have to be matched. Combining equations (1) through (5) one can obtain the scale factors for five dimensional parameters (major radius R, plasma current I_p, toroidal field B_t, plasma density n_e, and plasma temperature T_e) that are required to keep the dimensionless parameters constant when minor radius of the plasma a is changed. These scalings are summarized in Table 1.

Parameter	C-Mod	DIII-D	Scaling
R	.7 m	1.75 m	$\sim a$
a	.22 m	.55 m	$\sim a$
ε	.28	.28	
B_t	5.4 T	1.7 T	$\sim a^{-5/4}$
i_p	1 MA	.8 MA	$\sim a^{-1/4}$
n_e^{ped}	3×10^{20} m^{-3}	5×10^{19} m^{-3}	$\sim a^{-2}$
T_e^{ped}	600 eV	380 eV	$\sim a^{-1/2}$

Table 1. Scaling of plasma parameters required for dimensionless similarity. Typical C-Mod parameters (C-Mod column) are shown together with target DIII-D parameters (DIII-D column)

Another implication of the invariance of solutions of plasma equations is the similarity of the scalings of all timescales for plasma processes. A convenient timescale in magnetized plasmas is given by the cyclotron frequency, implying $\tau \sim 1/B$, and one can expect the other timescales to change in the same way. In fact it is easy to check that both the resistive diffusion time $\tau_R = \dfrac{a^2}{\eta}$ and the Alfven time $\tau_A = \dfrac{a\sqrt{4\pi m_i n_e}}{B}$ scale as $\dfrac{1}{B} \sim a^{5/4}$ if the scalings from Table 1 are applied. It was also shown in Ref. 11 that the quantity $B\tau_E$ is invariant when the dimensionless parameters are conserved if the energy confinement time τ_E is obtained from the solution of the basic plasma equations ignoring the effects of radiation by bremsstrahlung or impurities. Therefore we should expect the characteristic times of the plasma processes to scale as $a^{5/4}$ and scale the time bases for measured signals from different tokamaks accordingly.

Since the DIII-D tokamak has wider shape control capabilities than C-Mod, the typical shape of the C-Mod plasma was reproduced on DIII-D for the comparison experiments.

The goal of the experiment was to compare plasmas with matched local values of parameters that would characterize the H-mode edge. The natural choice in this case are the values on top of the H-mode pedestal. Shown in Table 1 are target parameters of the DIII-D plasma, including pedestal electron density and temperature, that had to be achieved to match a typical C-Mod H-mode plasma.

Traces of the programmed shape parameters and plasma current and magnetic field of one of the DIII-D discharges, together with a typical EDA C-Mod discharge, are shown in Fig. 1. In this and the following figures the values of DIII-D plasma parameters that scale with machine size (current and magnetic field in Fig. 1) and the time base for DIII-D discharge are scaled with the plasma minor radius (see Table 1). We were able to preprogram and maintain the DIII-D plasma shape almost exactly similar to typical C-Mod configuration . The upper triangularity of the DIII-D discharges is slightly higher than typical C-Mod value, restricting the number of C-Mod discharges that can be compared to the DIII-D plasmas. Matching plasma current and magnetic field led to an almost exact match of the safety factor.
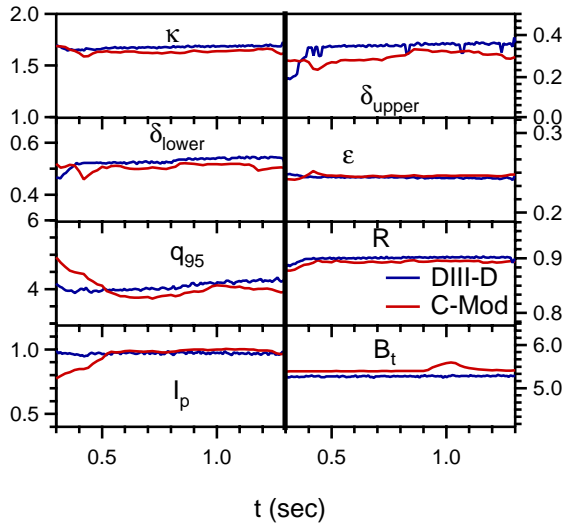

Fig.1 Traces of upper and lower triangularity ($\delta_{upper, lower}$), elongation (κ), inverse aspect ratio (ε), major plasma radius (R), edge safety factor (q_{95}), scaled plasma current ($I_p a^{1/4}$) and scaled toroidal magnetic field ($B_t a^{5/4}$). Time base for DIII-D discharge scaled as $a^{5/4}$. The excursion on the B_t trace for C-Mod is a preprogrammed 2% field sweep for scanning radial location of ECE measurement points

The required n_e^{ped} was obtained by an appropriate choice of the L-mode (Low confinement mode) target density in C-Mod; in DIII-D gas-puffing and cryo-pumping during the H-mode were also used to control the density.To obtain the pedestal temperature on DIII-D that would scale to the C-Mod value, the heat source was varied about a value obtained by appropriate scaling. The scaling of the required power source can be obtained by noting that the power flowing across a flux surface should scale as a product of the number of particles crossing the surface per unit time ($A n_e v$, where A is the area of the surface, and v is average particle velocity) and the average particle energy. Since the velocity scales as a square root of the particle energy (temperature) and $A \sim a^2$ one obtains $P \sim a^{-3/4}$ for the required scaling of the power flow across a flux surface. The pedestal heat source - power flowing across the separatrix into the scrape-off

layer - is largely determined by the auxiliary heating power. Therefore, in the first approximation, one can estimate the required heating power by scaling it in the same manner as the power across the separatrix. Since typical C-Mod ICRF heating power is between 2 and 3 MW, the required power for similar DIII-D plasma should be in the region from 1 to 1.5 MW. A series of discharges were run on DIII-D with various target densities and neutral beam powers to fill the range of pedestal parameter space required to match the typical C-Mod plasmas.
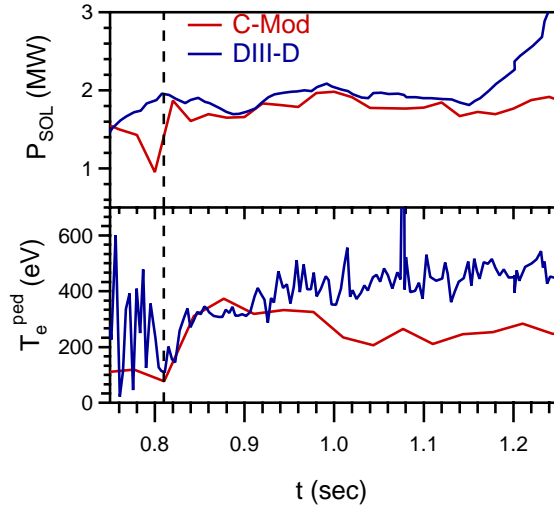

Fig. 2. Traces of calculated power flow across the separatrix (top) and measured pedestal temperature (bottom) for a pair of DIII-D and C-Mod discharges. The DIII-D parameters are scaled as $P_{SOL} * \left[\dfrac{a_{DIII-D}}{a_{C-Mod}}\right]^{3/4}$ and $T_e^{ped} * \left[\dfrac{a_{DIII-D}}{a_{C-Mod}}\right]^{1/2}$ Time base for DIII-D discharge scaled as $a^{5/4}$. Temperatures are similar for ~ 100 ms after the L-H transition (vertical dashed line), but deviate after that although the calculated P_{SOL} remain similar. See text for discussion

In Fig.2 the traces of calculated power flow across the separatrix are shown together with measured pedestal temperature for a pair of similar DIII-D and C-Mod discharges. The power flowing into the scrape-off layer is calculated according to

$$P_{SOL} = P_{in} + P_{ohm} - \frac{dW}{dt} - P_{rad} \qquad (6)$$

where P_{in} is the injected heating power ($0.8P_{ICRF}$ in C-Mod and neutral beam power in DIII-D), P_{ohm} is the ohmic heating power, dW/dt is the rate of change of the plasma stored energy and P_{rad} is the total radiated power. The radiated power was calculated from the signals of main chamber bolometers, excluding the volumes of lower and upper divertors on both tokamaks.

In this example, the normalized pedestal temperature is similar in both plasmas for approximately two confinement times after the L-H transition (vertical dashed line on the plots), corresponding to similar normalized P_{SOL}. After about 100 msec, the DIII-D pedestal temperature starts rising slowly, while the C-Mod T_e^{ped} decreases, although calculated power flux remains the same. The increase of T_e^{ped} in the DIII-D plasma is typical for the series of discharges in the experiment. It is accompanied by a change of the character of edge fluctuations, which will be discussed later in the paper. While the cause of the observed temperature rise is unclear, one of the possible hypotheses is that the edge parameters in those discharges are close to the threshold between two instabilities, and the change in the character of edge fluctuations

6

leads to the change of pedestal parameters. It should be noted that the increase of the temperature is followed by a sharp increase of the amplitude of the temperature fluctuations, as seen in Fig. 2.

In C-Mod, the gradual decrease of T_e^{ped} may be explained by a drop in efficiency of the ICRF heating. This efficiency depends strongly on the fraction of minority hydrogen ions in the plasma, and spectroscopic measurements show that the hydrogen fraction is increasing slowly after the RF source is turned on, possibly due to injection of hydrogen from the surfaces of the RF antennae. Therefore, the approximation of the constant heating efficiency (factor of 0.8 in front of RF power in (6)) is not valid and the real P_{SOL} decreases slowly after the L-H transition, leading to the observed change in the pedestal temperature.

Thus, by scanning the heating power source and plasma density we were able to obtain discharges with matching pedestal parameters (T_e and n_e). An example of two shots with similar pedestal dimensionless parameters is shown in Fig. 3. Time traces from the same DIII-D discharge as in Fig.2 are plotted together with traces from a different C-Mod discharge with input power slightly higher than the previously shown (3.5 MW instead of 3 MW) to obtain higher pedestal temperature. The dimensionless parameters are matched within the measurements errors during the H-mode (L-H transition at ~0.82 s) during the time period from 1 s to 1.2 s (between shaded regions in the graph). The pedestal heights (T_e^{ped} and n_e^{ped}) are obtained from the hyperbolic tangent fit to the measured pedestal profiles as described in [17,18,19]. The profiles were measured on both machines by edge Thomson scattering diagnostics (see Ref. 17 for C-Mod and Ref. 20,21 for DIII-D).
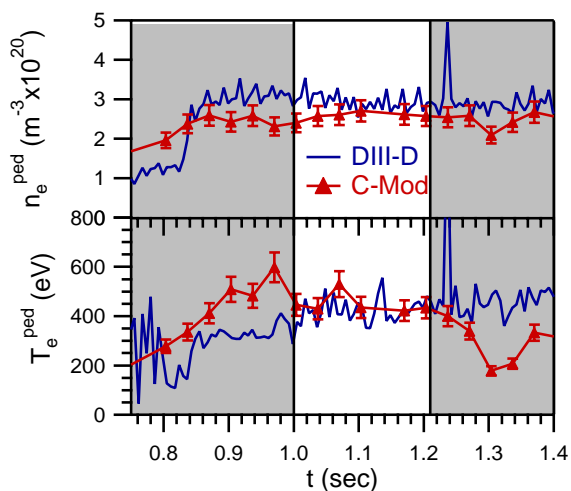

Fig.3 Time traces of pedestal density (top) and temperature (bottom) from similar DIII-D and C-Mod discharges. The values of T_e^{ped} and n_e^{ped} are obtained from the tanh fits of the Thomson profiles. Period when good similarity of pedestal parameters achieved is between the shaded regions. The L-H transition of both discharges is at ~ 0.8 sec. DIII-D data are scaled by machine size

III. Global plasma parameters in discharges with similar edges.

It is interesting to compare the core plasma parameters which were not scaled deliberately. Fig. 4 shows the time traces of the local electron temperature, density and pressure measured near the magnetic axis of the tokamak for the same discharges and time period as in Fig. 3.
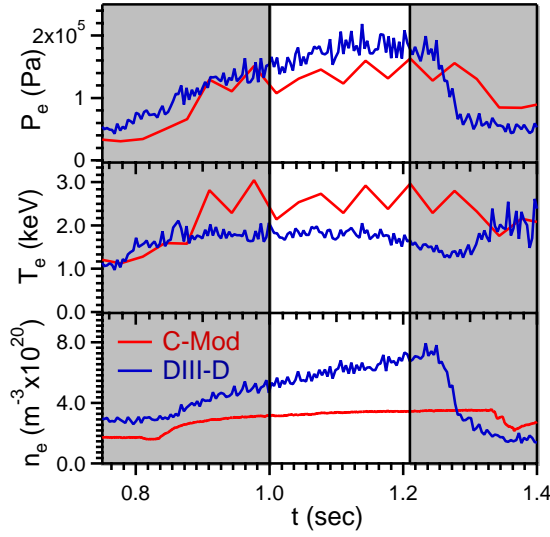
Fig. 4 Time histories of the local electron density, temperature and pressure P=knT measured near the plasma magnetic axis for discharges with similar edge parameters (see Fig. 3) DIII-D values are scaled with minor radius

It is clear, that although the pedestal parameters scale with the plasma radius, the core dimensionless parameters are not exactly similar in these two discharges. Several interesting features are apparent from the time histories of core n_e and T_e shown in the figure. In both machines at the L-H transition the pedestal density rises to its steady state level on a time scale faster than the confinement time and right after the transition a relatively flat density profile is formed in the core. On C-Mod this is followed by a core density rise on a time scale comparable to the confinement time and the core density reaches a steady state soon afterwards. In contrast, in the DIII-D discharge shown, as well as in all the discharges in the series, no fast core density rise is observed after the L-H transition. Instead, the core density increased slowly over the whole period of the H-mode, reaching the value of $\sim 1.5 n_G$, where n_G is the Greenwald density limit [22], $n_G = I_p / \pi a^2$. This high value of density is a possible cause of the back H-L transition at ~ 1.24 sec in the discharge presented in the figure (also observed in all the other discharges in the series).

The time history of the integrated number of particles in the plasma (DIII-D discharge) is shown in Fig. 5. The fast rise of the number of particles at the L-H transition corresponds to the fast growth of the density pedestal. During the period of the slow ramping, the rate of particles increase equals 23 A, which is equal, within reasonable error bars, to the rate of particle deposition by the heating neutral beam (24 A in this discharge). This suggests that without the additional particle source (neutral beam) the core density would remain at its initial value and the steady state H-mode would be obtained, as in the C-Mod discharge.

With the core plasma density higher in the DIII-D discharge and the input power approximately scaled with the minor radius, the core temperature of the plasma is somewhat lower than in C-Mod discharge. The value of the core electron pressure also does not appear to scale between the machines, with the scaled pressure in the DIII-D plasma being 25 – 35% higher than in C-Mod. Surprisingly, despite

8

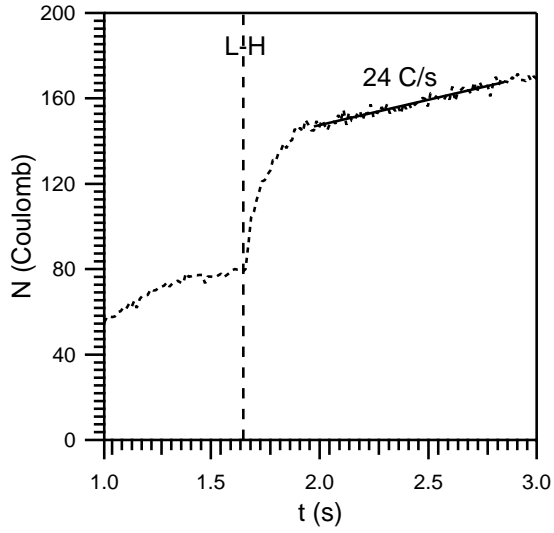relatively large differences in the values of the plasma parameters on axis, both the plasma stored energy

Fig. 5 Time history of integrated number of particles in the DIII-D discharge. The timebase is not scaled. Fast increase of N around 1.7 s represents the growth of density pedestal immediately after the L-H transition. The slower ramp up of N after 2 s is equal to therate of deposition of particles by the neutral beam

and the volume integrated β_t match closely in these two discharges. In Fig. 6 time traces of the stored energy (W), energy confinement time and volume averaged β_t of the C-Mod and DIII-D discharges are compared. For this comparison the DIII-stored energy is scaled as $a^{1/2}$ (taking into account that the stored energy is a volume integrated pressure profile $W \sim n_e T_e a^3 = a^{1/2}$) and the confinement time is scaled as $a^{5/4}$.
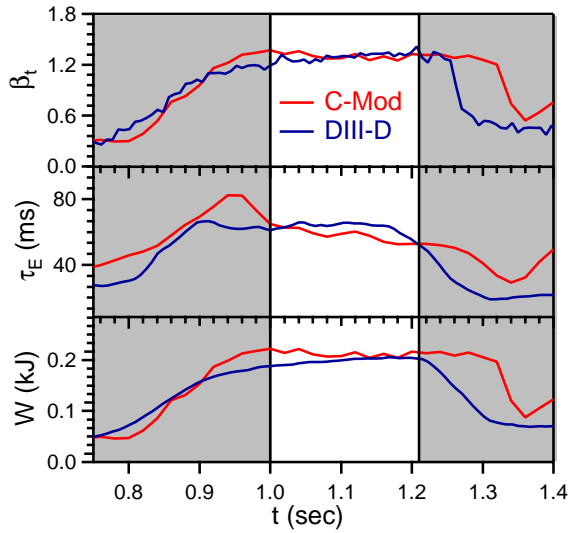

Fig.6 Time traces of volume integrated β_t, energy confinement time τ_E and stored energy W_{MHD} for C-Mod and DIII-D discharges with similar pedestal parameters (see Fig. 4). The plotted values of τ_E and W and the timebase for the DIII-D discharge are scaled with minor radius.

The close similarity of stored energy and β_t traces in discharges with similar dimensionless parameters on top of the pedestals supports the assumption that the global confinement is set by the pedestal parameters. Somewhat more surprising is the close match of the energy confinement times. The value of τ_E in the steady state discharge (when dW/dt=0) should scale as $a^{5/4}$ only if radiative losses of energy can be neglected or if radiated power scales in the same manner as the power flowing across the

separatrix. Although in both discharges the radiated power can not be neglected, it represents a relatively low fraction of the total input power ($P_{rad} \sim 0.2 P_{in}$). The difference between the total radiated power in the C-Mod and DIII-D discharges (if the P_{rad} for the DIII-D discharge is scaled as $a^{-3/4}$) is about $0.1 P_{in}$, which may account for approximately 10% difference in the scaled confinement times.

IV. Pedestal profiles.

As shown above, matching plasma parameters on top of the H-mode pedestals does lead to discharges with similar core transport and global confinement characteristics. A more immediate question is whether the pedestal profiles themselves are similar in these discharges, leading to similar MHD characteristics of the edge and, consequently, to similar H-mode character.

The width of the pedestal profiles, as defined by the results of the *tanh* fit to Thomson scattering data [17,20,21], fluctuates considerably even during a steady state phase of the discharge. Therefore, strictly speaking, to compare the profiles we should consider representative series of the pedestal parameters (height and width) measured throughout several similar discharges, rather than at a single time point. The comparison of such series is shown in Fig. 7, which shows pedestal widths for both machines plotted against corresponding pedestal heights. In this figure data from discharges with similar global plasma parameters and similar character of the H-modes on both tokamaks are shown.
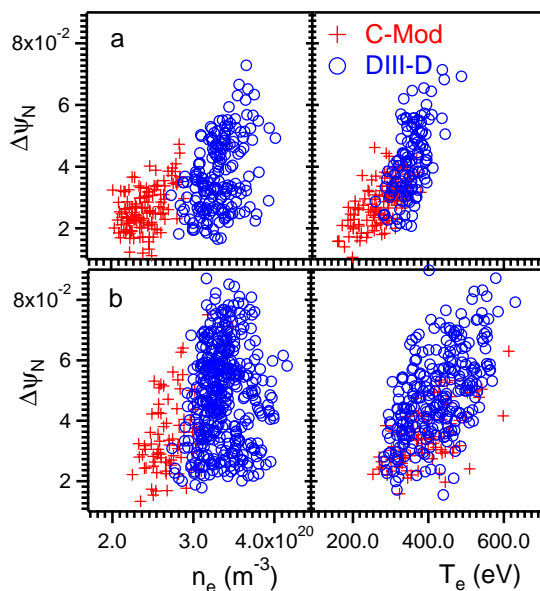

Fig.7. Pedestal width vs height for ELM-free (EDA) (a) and ELMy (b) phases of the discharges. Pedestal heights from DIII-D discharges are scaled with a. Pedestal widths in normalized flux coordinates are obtained by mapping the measured profiles to the flux surfaces using EFIT

Only discharges with upper triangularity between .32 and .36, and lower triangularity between .5 and .54 are used. The points from C-Mod discharges with plasma current between .97 MA and .99 MA, corresponding to the scaled plasma current in the DIII-D series, are chosen. The measured electron temperature and density profiles from both tokamaks are mapped to the normalized poloidal flux

coordinates using the equilibrium reconstruction code EFIT. The widths in fig.7 are shown in these flux coordinates. The heights of the DIII-D pedestals are scaled with the ratio of C-Mod and DIII-D minor radii. In the majority of the discharges in the DIII-D series an ELM-free H-mode period was observed reminiscent to the C-Mod EDA H-mode (as will be discussed in the next section). Fig. 7a shows the comparison of the C-Mod EDA pedestal parameters with the DIII-D parameters during these ELM-free periods. Fig. 7b represents the comparison of DIII-D and C-Mod pedestals in H-mode with small grassy ELMs (see next section).

It is clear that the widths of both temperature and density pedestals fluctuate considerably at a given pedestal height, and the amplitude of these fluctuations is larger in the ELMy discharges than in EDA-like discharges. We were able to achieve good temperature pedestal match in almost all cases – plots of T_e^{ped} vs $\Delta\psi_N$ (pedestal width in normalized flux coordinates) overlap almost completely – by fine tuning the input heating power in DIII-D discharges. The accurate density control proved to be more difficult and matching density pedestals were obtained only in a narrow range around 3×10^{20} m^{-3} of the C-Mod density. It is seen, however, that in the region where heights of the density pedestals match on both tokamaks, the pedestal width fluctuates between the same values. Also, the envelop of the height vs width dependencies is similar for both machines. In particular, there is a clear tendency of the upper boundary of density pedestal width to increase with the pedestal height. The same trend is also observed for the temperature pedestal.

Analysis of measured pedestal profiles shows that the fluctuation of the pedestal width is greater than the data scatter expected from statistical and instrumental errors. The fluctuations are possibly caused by the quasi-coherent edge localized mode that exists in the EDA H-mode [23,24], and by the effect of ELMs on the pedestal structure during ELMy phases. Because of these fluctuations we clearly can not expect to find the exact match of the pedestal profiles on both machines even if the edge plasma physics is absolutely similar. However, the absence of a discontinuity between two measured width vs heights distributions suggests that certain degree of similarity is achieved in the discharges under consideration. It becomes even more apparent when individual profiles are considered. Fig. 8 shows the comparison of edge temperature and density profiles from both tokamaks for two cases – one representing the time slice when both width and heights of the pedestals match (Fig. 8a), and the other showing the time point when pedestal densities are similar but widths are in the opposite limits of the range of fluctuations on Fig. 7a (Fig. 8b). The profiles from C-Mod are shifted slightly (<0.02 of ψ_N) to overlap the profiles for comparison purposes. The shift is smaller than the known EFIT mapping error of $\sim 3\%$. It should be noted that the mapping error affects only the absolute position of the pedestal relative to the separatrix, but not the pedestal width. The accuracy of the measurements of the width is determined mainly by the spatial resolution of the diagnostics.

It is seen from Fig. 8a that pedestal profiles on C-Mod and DIII-D can be identical within the measurements errors. In the density profiles on Fig. 8b the difference in the width of the scaled DIII-D profile is apparently caused by density fluctuations at the outer half of the pedestal.
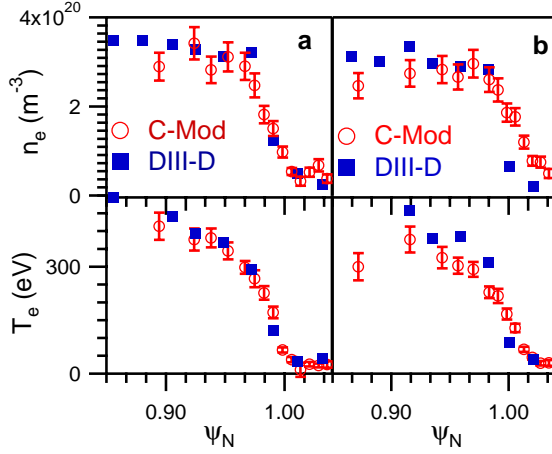
11

Fig.8 Examples of pedestal profiles representing matching density points on Fig 7a (a) and a pair of points with similar density pedestal heights but different widths (b). DIII-D T_e and n_e are scaled with machine size

Thomson scattering, which is used to measure the pedestal profiles on both machines, provides a snapshot of the edge profiles within the duration of the laser pulse (~ 10 ns). If the observed scatter in the pedestal width is caused by the edge fluctuation, averaging the profiles over several recorded time points should reduce the effect of plasma fluctuations on the measured width and height. Fig. 9 shows such averaged profiles for two discharges with matching pedestal density height, shown in Fig. 3. The profiles are averaged on both machines within the time range where the n_e^{ped} are similar (6 time slices from C-Mod and 30 time slices from DIII-D). Although the individual profiles from these discharges can have quite different width, the averaging produces very similar profiles on both tokamaks.
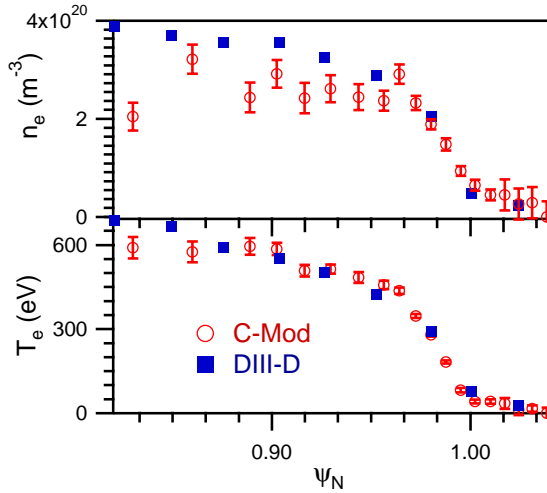

Fig.9 Time averaged profiles from C-Mod and DIII-D discharges with matched density pedestal height (see Fig. 3). DIII-D T_e and n_e are scaled with machine size

General considerations of power and particle balance at the edge suggest that the density profiles are formed as a result of equilibration of the charged particles transport out of the plasma and the neutral flux into the plasma, which forms the ion source in the barrier region. Independent of a particular model of ion diffusion and neutral penetration, the continuity equation should be satisfied:

$$\nabla \cdot \vec{\Gamma} = S \qquad (7)$$

where Γ is the ion flux and S is the local ion source (a steady state with $dn_e/dt=0$ is assumed)

Therefore, if we assume the diffusive flux $\Gamma = D\nabla n_e$, where D is a diffusion coefficient, the width of the pedestal profiles should be determined by both plasma transport and neutral penetration characteristics that define the spatial extent of the source S. The latter should be different in different machines because it depends on both neutral source configuration and absolute values of plasma temperature and density rather than on dimensionless plasma parameters. A crude estimate of the neutral penetration length can be made as:

$$L = \sqrt{\frac{kT_n}{m_i \xi_i \left(\xi_i + \xi_{cx} \right)}} \frac{1}{\overline{n}_e} \qquad (8)$$

where T_n is the neutral temperature, which is assumed constant, $\overline{n}_e$ is the average electron density, ξ_i is the ionization rate, ξ_{cx} is the charge-exchange rate , and m_i is the ion mass [25,26]. Although this estimate is based on strong simplifying assumptions ($T_i=T_n=$const), it allows us to establish a possible scaling of the characteristic neutral penetration length with the machine size. If pedestal density and temperature are scaled to match the dimensionless parameters, the parameter L should change as $a^{7/4}$ (assuming constant atomic processes rates, which are changing weakly in the temperature range from 100 to 1000 eV [27]).

In fact, the average measured density pedestal profiles are similar in normalized flux coordinates, which means that the measured pedestal width in similar discharges on both tokamaks scales as the plasma radius, which is a significantly weaker scaling than the $a^{7/4}$ expected from the neutral penetration model. The observed increase of the density pedestal width with the pedestal height is also opposite to the inverse dependence of the penetration length on the pedestal density that follows from (8). (It should be noted, however, that it is possible that the observed widening of the pedestal with increasing density may be caused by increasing fluctuation amplitude).

Several possible explanations of this seeming contradiction between the experimental results and the continuity equation can be offered. If the major fueling sources on both machines are situated in different poloidal locations (i.e midplane fueling on C-Mod and divertor fueling on DIII-D), the difference in flux expansion in those locations can lead to matching neutral penetration lengths in flux coordinates. This model is discussed in details in [28]. It is also possible that a pinch term has to be included in (8) that balances the diffusion and ion source terms. At last, the ion transport may not be diffusive or the diffusion coefficient may not scale with the plasma parameters but adjusts itself to the neutral source to maintain certain electron density gradient in the transport barrier region (a critical gradient transport model). Unfortunately, no experimental evidence is available at the moment to support or disprove any of the above models, so the solution of this problem has to be the subject of future studies.

V. Edge fluctuations

The dimensionless identity implied by the observed profile matching should extend to other plasma behavior as well. We should expect similar edge stability characteristics, and similar character of the edge fluctuations in the matched discharges.

In Figure 10 the time traces of pedestal temperature, density, volume integrated β and D_α intensity from one of the series of the DIII-D discharges are compared to two different C-Mod shots. The DIII-D data and time base are scaled with the minor radius as above. The C-Mod discharges are different only by the amount of the input power. The discharge that has power flow across the separatrix which scales to the DIII-D value (see Fig. 2) is shown in Fig. 10a. This discharge is a typical example of the EDA H-mode [23,24]. The other discharge (Fig. 10b) has higher auxiliary heating power (3.5 MW instead of 3 MW) that results in higher pedestal temperature and represents a case of ELMy H-mode.
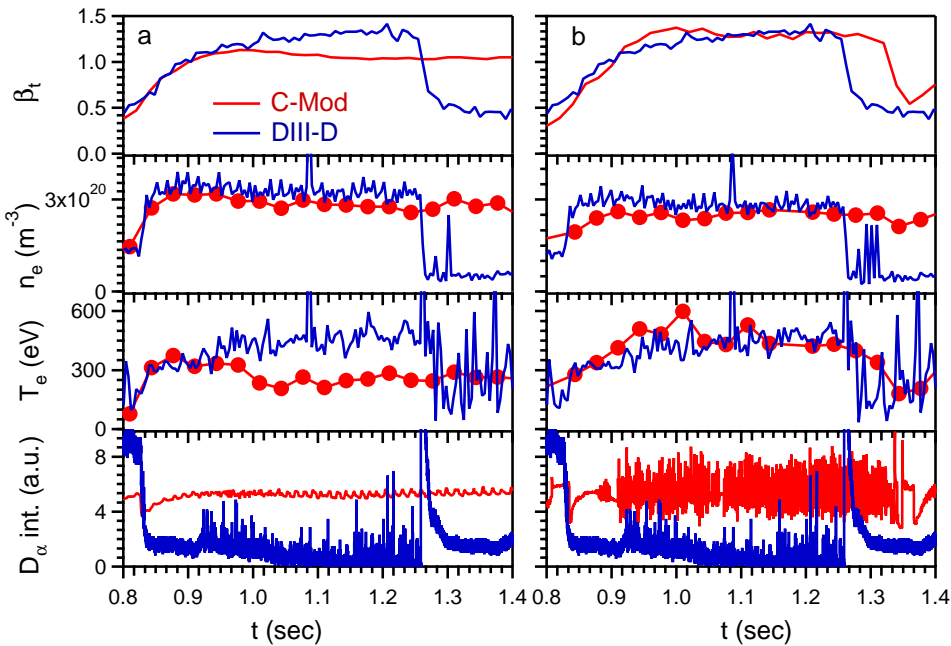

Fig. 10. T_e and n_e pedestal heights, volume integrated beta and D_α signal for a DIII-D discharge and two C-Mod discharges with different pedestal temperatures. Similar pedestal and global parameters correspond to similar edge fluctuations – EDA like regime for low T_e (left panel, .82 - .92 s) and small ELMs for higher T_e (right panel, .92 to 1.25 s). DIII-D data are scaled by machine size

As pointed out in section II, the pedestal temperature and density of the DIII-D discharge match those of the C-Mod EDA discharge at the beginning of the H-mode. The D_α signal of the DIII-D shot indicates an ELM-free period after the L-H transition, followed by small, high frequency ELMs. During the

ELM-free period of the DIII-D discharge, when pedestal parameters match the corresponding C-Mod values, a quasicoherent mode is observed, localized within the DIII-D pedestal (Fig. 11b)   It is characteristic for all the DIII-D discharges of the series, that after a brief ELM-free period with relatively constant pedestal temperature and density, the pedestal temperature starts to increase (although the input power is kept constant) and at the same time the transition to grassy ELMs is observed. It is possible that this transition is caused by increasing β. It is seen from Fig. 10 that β_t of the DIII-D plasma exceeds the C-Mod value starting from about the point of the transition. This increase at constant input power is probably caused by ramping up of the core plasma density (see Fig. 4). A possible explanation of the transition to ELMy regime would be that rising β leads to changes in equilibrium (increasing Shafranov shift) that destabilize edge modes exhibiting themselves as small ELMs. Then the heat transport at the edge changes and the pedestal temperature increases. Appearance of the small ELMs also seems to prevent the further increase of beta. A change of slope in the rise of beta appears around the time of transition to the ELMy regime (t=.93 s, Fig. 10a) and soon β_t reaches a steady state value of $\sim 1.3\%$

The ELMy period of the DIII-D discharge is very similar to the ELMy C-Mod discharge (Fig. 10b), although in C-Mod plasma the high values of β and of the pedestal temperature are due to higher input power. The C-Mod discharge shown in Fig. 10b has pedestal temperature and density matching those of the ELMy period of the DIII-D discharge. Note that both time history and absolute value of β also match. The ELMy period in C-Mod discharge is preceded by the short EDA period of the length similar to the DIII-D ELM-free period, that lasts until β_t increases above the value of ~ 1.1 . The ELMs seen in D_α signal are similar – small, irregular, of higher frequency than regular type I ELMs.

Fig. 11 shows the edge fluctuation spectra from C-Mod (b) and DIII-D discharges (a) together with the D_α trace. The C-Mod discharge represents the typical case of a quasicoherent mode observed in EDA H-mode. The C-Mod spectra is measured with a magnetic probe. The DIII-D spectrum is observed by a 32 kHz edge reflectometry channel that monitors the bottom of the pedestal.

The quasicoherent mode observed in the C-mod discharge (Fig. 11b) is a signature of the enhanced D_α H-mode (EDA), which is typical for C-Mod plasmas under most operational conditions. It was shown previously, that this mode is responsible for the enhanced impurity transport in EDA [23,24]. It is typical for the QC mode to start at a frequency around 250 kHz and then slow down to frequencies in the range from 100 to 50 kHz, as shown in Fig 11b. Since the observed frequency of the mode is a sum of plasma rotation frequency and the mode frequency in the plasma's reference frame, this change in the mode frequency is attributed to the change of the plasma rotation velocity after the L/H transition.

The DIII-D spectrum shows that a similar mode exists in the edge of the DIII-D plasma in the phase preceding the appearance of small ELMs. The mode seen in the DIII-D spectrum (Fig. 11a, 0.55 – .62 s) has several characteristics similar to the C-Mod QC mode. First of all, the measured poloidal wavenumber of the mode scales to the C-Mod value. The typical values of k_θ for C-Mod are 1.2 – 1.5 cm^{-1} at the midplane. The results of the Beam Emission Spectroscopy (BES) measurements on DIII-D show the values of k_θ between 0.52 and .63 cm^{-1} at the midplane. For comparison, with normalization to the ratio of

15

minor radii a_{DIII-D}/a_{C-Mod}=.55/.22 these values become 1.3 – 1.6 cm^{-1}, almost exactly matching the k_θ measured on C-Mod. The poloidal variation of k_θ observed on C-Mod is in agreement with the expected variation of the poloidal wavenumber of a ballooning mode which follows [29] from the conservation of toroidal mode number and the relation k_ϕ=n/R. The poloidal wavenumber, k_θ, for ballooning modes (for which $\mathbf{k \cdot B}$≈0, or $k_\theta B_\theta$≈$-k_\phi B_\phi$) varies within a flux surface as $k_\theta(\theta_1)/k_\theta(\theta_2)$≈ $[B_\theta(\theta_2)R_2^2]/[B_\theta(\theta_1)R_1^2]$. Thus k_θ ~ 2.6 cm^{-1} measured by PCI diagnostics on top of the C-Mod plasma translates into the values ~ 1.2 cm^{-1} measured by the magnetic probe at the midplane. Similar poloidal variation is observed in DIII-D discharges, where probe measurements 20 cm below the midplane give k_θ =.73 cm^{-1}, which scales to smaller values measured at the midplane.
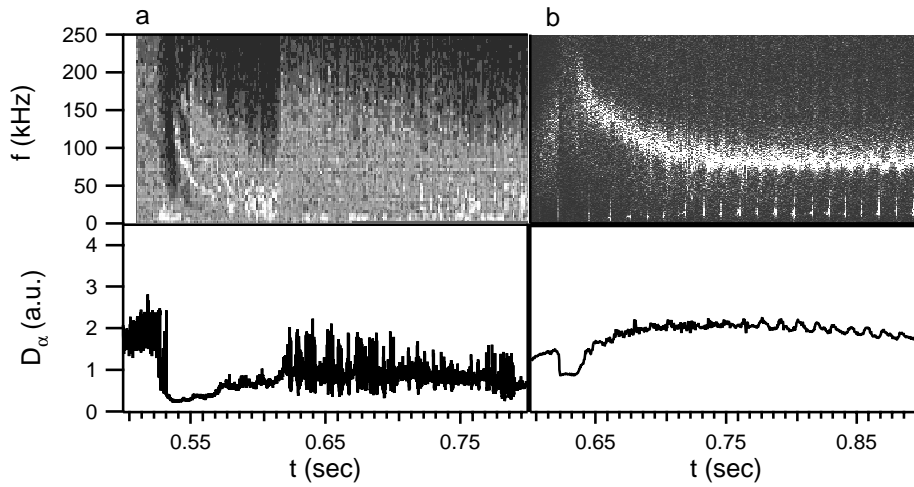

Fig. 11 Edge fluctuation spectra from a C-Mod EDA discharge and one of the DIII-D discharges from the identity experiment both showing a quasicoherent mode at the edge appearing shortly after the L/H transition. In DIII-D case the mode is replaced at 0.62 s by broadband fluctuations representing small ELMs. The frequency and timebase for DIII-D data are scaled with minor radius

It should be noted, that in contrast to the C-Mod QC mode, which is always observed as a single frequency mode, the DIII-D mode consists of several quasicoherent frequencies. Above the peak at the base frequency of 12 – 13 kHz, the peaks around 25, 35, 55 and 65 kHz are observed. Typical frequency of the C-Mod QC mode changes between 50 and 150 kHz depending on plasma conditions. If we assume that the mode frequency should scale in the same way the other characteristic times scale, then the scaled value of the mode frequency in the DIII-D discharge should be $12 \bullet \left[\dfrac{a_{DIII-D}}{a_{C-Mod}} \right]^{5/4} = 38 \text{kHz}$ Although the multiple frequencies of the DIII-D mode suggests certain differences between the C-Mod and DIII-D discharges, the different values of the measured frequencies (38 kHz on DIII-D as opposed to 100 kHz on C-Mod) do not necessarily imply a difference in the underlying physics. The frequency of the mode as measured in the

laboratory frame of reference is a sum of the frequency in the plasma frame of reference and the frequency of the plasma rotation. Therefore, the observed lack of scaling of the mode frequencies may just indicate different plasma rotation velocities for both machines.

Conclusion.

H-modes with similar characteristics were observed on tokamaks of different sizes in plasmas with similar shape and local edge dimensionless parameters. It was shown that similarity of the plasmas in the H-mode pedestal region leads to similar global plasma characteristics (global confinement and transport) even when auxiliary heating mechanisms and fueling mechanisms are different. Although in the DIII-D discharges additional fueling by the neutral beam altered the core density and temperature profile significantly, global plasma characteristics such as volume integrated beta and stored energy matched well in the discharges with similar pedestal parameters and different heating mechanisms (ICRF on C-Mod and neutral beam on DIII-D).

Not only were the dimensionless plasma parameters matched at the top of the pedestal, but they were also found to be similar in the steep gradient region of the H-mode transport barrier. These results seem to indicate that the model based on balancing purely diffusive ion transport flux and the ion source resulting from neutrals penetrating into the plasma across the separatrix can not be used to fully describe the pedestal physics. However, the large fluctuations of the pedestal width even during the steady state phase of the discharge can effectively mask the differences in the pedestal structure and a correlation of the pedestal width with its height as predicted by the model. In any case, this model cannot be fully assessed without better knowledge of the poloidal distribution of fuelling in the two machines than now exists. Further studies of the physics of neutral penetration and plasma transport in the pedestal region are necessary to make any definite conclusions on the subject.

When the dimensionless plasma parameters were matched at the edges of C-Mod and DIII-D, similar physics phenomena were observed in the two machines, as shown in two different ways. When the pedestal parameters in DIII-D matched the conditions for the EDA H-mode in C-Mod, an edge density fluctuation was seen in DIII-D that had very similar characteristics to the quasi-coherent mode observed in C-Mod. In particular, the wavenumbers and locations of the fluctuations in the two machines showed relationships expected from matching of the dimensionless parameters. Thus, there is little doubt that the quasi-coherent mode was produced in DIII-D. As a second example of similar physics phenomena, with the dimensionless parameters matched at slightly higher values of pedestal temperature and beta, the quasi-coherent mode in both machines was replaced by broadband fluctuations, corresponding to small irregular ELMs. These results show that the techniques of dimensionless identity provide a powerful way to unite pedestal studies in different machines, operating perhaps at very different engineering parameters.

Acknowledgement.

References.

[1] I. H. Hutchinson *et. al*., Physics of Plasmas 1, 1511, (1994)

[2] J. L. Luxon, Nuclear Fusion 42, 614, (2002)

[3] W. Suttrop, M. Kaufmann, H. J. de Blank *et. al.*, Plasma Phys. Controlled Fusion, 39, 2051, (1997)

[4] M. Greenwald, R. L. Boivin, F. Bombarda *et. al.* Nucl. Fusion , 37, 793, (1997)

[5] A. E. Hubbard, B. Lipshultz, D. Mossessian et. al., Proceedings of 26th EPS Conference on Controlled Fusion and Plasma Physics, Maastricht, vol. 23J, 13, (1999)

[6] D. Mossessian, A. E. Hubbard, E. Marmar *et. al.* Plasma Phys. Controlled Fusion. , 42, A255, (2000)

[7] D. Mossessian, J. W. Hughes, A. E. Hubbard *et. al.* Proceedings of 27th EPS Conference on Controlled Fusion and Plasma Physics, Budapest, Hungary, 386(2000),

[8] J. P. Christiansen, *et. al.* Proceedings of 17th IAEA Fusion Energy Conference, Yokohama, Japan, (1998)**?**

[9] J. G. Cordey, B. Balet, D. Campbell *et. al.*, Plasma Phys. Control Fusion, 38, A67, (1996)

[10] B. B. Kadomtsev, Sov. Journal Plasma Phys., 1, 295, (1975)

[11] J. W. Connor, J. B. Taylor, Nucl. Fusion, 17, 1047, (1977)

[12] K. Lackner, Comments Plasma Phys. Controlled Fusion, 13, 163, (1990)

[13] T. C. Luce, C. C. Petty, Physica Scripta, 52, 444, (1995)

[14] F. Ryter, F. Imbeaux, F. Leuterer, *et. al.* Phys. Rev. Letters, 86, 5498, (2001)

[15] L. D. Horton, J. P. Christiansen, J. Lingertat *et. al*. Plasma Phys. Controlled Fusion, 41, B329, (1999)

[16] M. Kotshenreuther, W. Dorland, M. A. Beer , G. W. Hammet Phys. Plasmas, 2, 2381, (1995)

[17] J. W. Hughes, D. A. Mossessian, A. E. Hubbard, Rev. Sci. Instrum., 72, 1107, (2001)

[18] R. J. Groebner, T. N. Carlstrom, Plasm Phys. Controlled Fusion, 40, 673, (1998)

[19] R. J. Groebner *et. al.*, 1996 Fusion Energy (Montreal) v. 1 (Vienna:IAEA), 867, (1996)

[20] T. N. Carlstrom, G. L. Campbell, J. C. DeBoo *et. al*.,Rev. Sci. Instrum, 63, 4901, (1992)

[21] B. Bray , C. Hsieh, T. N. Carlstrom *et. al.*, Rev. Sci. Instrum, 72, 1115, (2001)

[22] M. Greenwald, J. L. Terry, S. M. Wolfe, *et. al.*, Nucl. Fusion, 28, 2199, (1988)

[23] M. Greenwald., R. Boivin, P. Bonoli *et. al.* Phys. Plasmas 6, 1943, (1999)

[24] A. E. Hubbard, R. L. Boivin, R. S. Granetz *et. al.* Phys. Plasmas 8, 2033, (2001)

[25] B. Lehnert, Nucl. Fusion, 23, 1327, (1983)

[26] M. B. Tendler, O. Agren, Phys. Fluids 25, 1037, (1982)

[27] R. K. Janev, W. D. Langer, K. Evans Jr., D. E. Post Jr., "Elementary processes in Hydrogen-Helium Plasmas" (Springer-Verlag, Berlin, Heidelberg, 1987)

[28] R. J. Groebner, M. A. Mahdavi, A. W. Leonard *et. al.*, Phys. Plasmas, 9, 2134, (2002)

[29] J. Myra, D.A. D'Ippolito, X.Q. Xu, and R.H. Cohen, Phys. Plasmas **7**, 4622, (2000)